JOURNAL OF AIRCRAFT
Vol. 37, No. 1, January–February 2000

Engineering Notes

ENGINEERING NOTES are short manuscripts describing new developments or important results of a preliminary nature. These Notes cannot exceed 6 manuscript pages and 3 figures; a page of text may be substituted for a figure and vice versa. After informal review by the editors, they may be published within a few months of the date of receipt. Style requirements are the same as for regular contributions (see inside back cover).

Numerical Analysis of Advanced Fighter Auxiliary Power Unit Exhaust Impingement

Philip M. Cali*
U.S. Air Force Research Laboratory,
Wright–Patterson Air Force Base, Ohio 45433-7913

Introduction

A THREE-DIMENSIONAL, viscous, computational fluid dynamics (CFD) analysis of the exhaust flow associated with the auxiliary power unit (APU) of an advanced fighter aircraft was conducted. Calculations were performed to investigate the level of surface heating on the fuselage adjacent to the APU exhaust port.

The present aircraft's APU consists of a small turbine engine located inside the upper surface of the fuselage (Fig. 1). During a main engine flameout, two small doors (which are normally flush with the fuselage surface), open to initiate the APU's operation (Fig. 2). Attached to the first door is a scoop that diverts a flow of air down through the fuselage and into the APU plenum. After compression and combustion, the high-temperature effluents are exhausted upward into the external flowfield through the APU exhaust port.

The current analysis investigates APU exhaust impingement onto a region of composite structure inboard of the APU exhaust port. The material in this region was not designed to withstand extreme temperatures and is susceptible to heating related damage during periods of prolonged APU operation. It was proposed that the inboard heat transfer to the fuselage could be minimized by relocating a small high-pressure surge line from its original position directly downstream of the APU exhaust port to a position directly inboard of the APU exhaust port (Fig. 2). In this way, the flow discharged by the surge line could be used to redirect the hot effluents downstream and away from the vulnerable area. The current numerical study was designed to investigate the impact of the surge line relocation on the APU exhaust flow.

Numerical Procedure

The three-dimensional, compressible, mass-averaged Navier–Stokes equations were solved to predict the flow about the two APU configurations. The computer code, FDL3DI, which incorporates a two equation (κ–ε) turbulence model, was used in all calculations. The code was based on the implicit approximately factored finite difference algorithm of Beam and Warming.[1] A first-order implicit temporal discretization and a second-order spatial discretization were employed. Common forms of implicit and explicit nonlinear artificial dissipation were implemented to augment stability using proven values of the damping coefficients. Computational efficiency was enhanced by solving the implicit portion of the factored equations in diagonalized form. The (κ–ε) equations, which were developed by Jones and Launder,[2] were decoupled from the Navier–Stokes equations by lagging the values of the turbulence variables behind the other dependent variables by one time step. A thorough description of the code's numerical algorithm as well as citations to previous analyses conducted using FDL3DI are given in Ref. 3.

Grid Generation

Because of the complexity of the geometry, the Chimera domain decomposition methodology was employed. Information was passed between adjacent meshes using a trilinear interpolation approach at the boundaries of overlapping domains. Taking advantage of the modular nature of the Chimera technique, an existing system of computational grids constructed about the fighter aircraft was used as the starting point for the current analysis. A set of APU meshes was then embedded into the original fighter system.

In its entirety, the original grid system consisted of seven meshes constructed on one-half of the spanwise–symmetrical fighter. Overlapping grids were constructed for each of the various components of the aircraft (nose, fuselage, engine inlet, wing, vertical tail, and horizontal tail). This system was then embedded into a far-field background mesh that extended five root chord lengths ahead and behind the aircraft and two root chord lengths outward from the wing. Clustering of grid lines near all surfaces was accomplished using a hyperbolic tangent distribution function with a surface spacing of $\Delta\eta_s/c = 2.5 \times 10^{-5}$. This value was based on a compromise between reasonable $y+$ estimates, memory requirements, and computational efficiency.

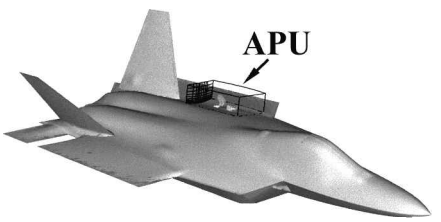

Fig. 1 APU location on the upper fuselage.

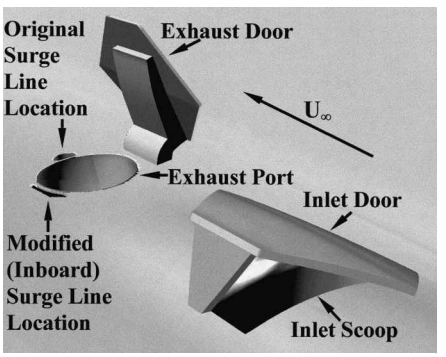

Fig. 2 Deployed APU with both surge line locations.

Presented as Paper 98-0770 at the AIAA 36th Aerospace Sciences Meeting, Reno, NV, 12–15 January 1998; received 7 February 1998; revision received 27 June 1998; accepted for publication 1 July 1998.

*Aerospace Engineer, CFD Research Branch, Flight Vehicles Directorate. Member AIAA.

Solutions to the complete seven-grid fighter configuration were classified and required special computing facilities. This restriction was severely limiting because of the unavailability of such machines. To expedite the APU analysis, an unclassified subset of the original seven-grid system, in which the wing and horizontal tail meshes were removed, was employed. The resulting five-grid system contained approximately 900,000 points.

A system of APU grids was next embedded into the clean aircraft system. A total of 17 additional meshes were necessary to adequately model the APU geometry. Because of difficulties establishing communications in the boundary layer, the APU geometry was defined using a system of meshes in which the surface grid point spacing was relaxed. These meshes were then embedded within an H–H viscous background mesh that extended outward from the fuselage surface with the same resolution as the clean aircraft grids ($\Delta\eta_k/c = 2.5 \times 10^{-5}$). While the nonviscous grids were responsible for defining the APU surfaces, the APU background mesh was responsible for providing adequate resolution on the fuselage surface as well as sufficient overlap with the outer aircraft grids. This compromise, although not ideal, was deemed necessary to make the solution manageable in a realistic time frame. The entire set of 22 grids (fighter + APU) contained approximately 2.3 million grid points. An in-depth description of all the grids (including figures) is provided in Ref. 3.

Boundary Conditions

A 1-g return flight ($M = 0.7$, $\alpha = 2.0$ deg, $Re = 4.6 \times 10^7$) after a successful main engine restart was selected to represent the condition associated with the most severe APU impingement damage. Freestream values were set using a standard hot-day model and the full-scale wing root chord (c) was chosen as the reference length.

Characteristic boundary conditions were used at all far-field boundaries. On solid surfaces, no-slip, adiabatic wall, and zero normal pressure gradient conditions were specified. A symmetry condition was enforced at the inboard spanwise boundary and a simple flow-through extrapolation was implemented at the main engine inlet. Based on APU operating information, a mass outflow condition was imposed at the APU inlet and both mass inflow and temperature conditions were set at the APU exhaust and surge line.

Clean Fighter Configuration

Although time constraints precluded a formal grid resolution study, efforts were made to validate the unclassified configuration as adequate for providing the background flow for the APU analysis. Calculations using the five-grid system were first conducted without the additional APU meshes and the results compared to wind-tunnel test data.[4] Unfortunately, experimental data were only available for the clean aircraft configuration without deployed APU.

The validation test conditions ($M = 0.6$, $\alpha = 0.0$ deg, $Re = 4.6 \times 10^6$) were chosen from the available test data to most closely match those of the 1-g APU test case discussed in the previous section. Convergence was determined by monitoring the respective force coefficients. Flowfield residuals were reduced five orders of magnitude in approximately 3000 iterations. This level of convergence required approximately 35 CPU hours on a Cray C-90.

Calculated values of $y+$ on the fuselage surface were typically about 2.5. Such values are generally considered too large to establish the quantitative accuracy of a solution. However, given the scope of the current work, which was primarily focused on predicting trends, the reported $y+$ values were judged acceptable.

To evaluate the quality of the calculation, pressure predictions on the fuselage surface were compared to the pressure data from the wind-tunnel test. Color-contour pressure comparisons are presented in Ref. 3. A comparison of the pressure distribution in the region of the APU is shown in Fig. 3. The line plots begin at the aircraft's centerline and extend outward in the spanwise direction. Because of the good agreement of these data, the five-grid, unclassified configuration was judged acceptable for the present APU study. It should be noted, however, that although the pressure comparison served as a good diagnostic check to confirm that the solution was reasonable, it should not be interpreted as an indicator of the quantitative accuracy of the more difficult to predict quantities such as skin friction and heat transfer.

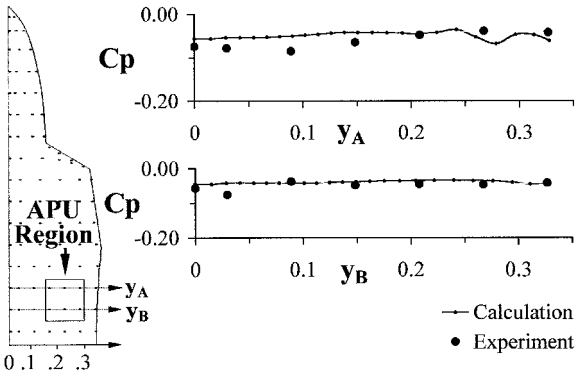

Fig. 3 Clean aircraft spanwise pressure coefficient comparisons in the region of the APU.

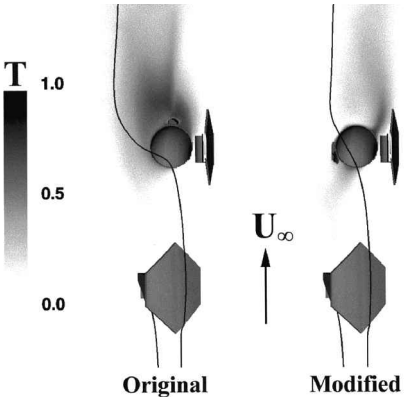

Fig. 4 Nondimensional temperature contours on the fuselage surface.

APU Test Cases

The APU test cases were calculated with the surge line in both its original and modified locations. Convergence was ascertained by monitoring the force coefficients as well as the temperature distribution on the surface adjacent to the APU. Although the flow was inherently unsteady because of a large separation region behind the APU inlet door, solutions converged to a pseudosteady condition in which the maximum variation in surface temperature was reduced five orders of magnitude. This level of convergence was achieved in approximately 10,000 iterations and required 300 CPU hours on a Cray C-90 for each case.

Figure 4 shows temperature distributions and characteristic particle traces in the region of the APU for both cases. To declassify the solution, the temperature scale was normalized from 0 to 1. In the baseline case, the interaction between the external flow, the hexagonal exhaust door, the subsonic APU exhaust flow, and the supersonic flow emitted from the downstream APU surge line creates a large inward component of the flow (illustrated by a particle trace emanating from the tip of the inlet door). This inward flow sweeps the hot exhaust gases inboard and results in a high-temperature region on the surface adjacent to the APU exhaust port. The relocation of the surge line flow to the inboard position diverts the exhaust flow downstream, away from the vulnerable inboard area. Consequently, the extent of the surface temperature footprint inboard of the APU exhaust port in the modified case is vastly reduced.

Although a grid resolution study would be desirable to assess the quantitative accuracy of the solution presented, the trends identified corroborated the results of previous APU exhaust impingement analyses. In this way, the current CFD investigation served (in a timely fashion) to reduce the overall risk associated with the proposed design modification.

References

[1]Beam, R., and Warming, R., "An Implicit Factored Scheme for the Compressible Navier–Stokes Equations," *AIAA Journal*, Vol. 16, No. 4, 1978, pp. 393–402.

[2]Jones, W. P., and Launder, B. E., "The Calculation of Low-Reynolds-Number Phenomena with a Two-Equation Model of Turbulence," *International Journal of Heat and Mass Transfer*, Vol. 16, No. 6, 1973, pp. 1119–1130.

[3]Cali, P. M., "Numerical Analysis of Advanced Fighter Auxiliary Power Unit (APU) Exhaust Impingement," AIAA Paper 98-0770, Jan. 1998.

[4]Bryant, M. D., Arendt, L. L., and Hobbs, R. W., "Wind Tunnel Test of a 0.10-Scale Pressure Model With and Without Stores," AEDC-TSR-93-P3, Feb. 1993.

Improvement of a Wing's Aerodynamic Efficiency Using Coanda Tip Jets

R. G. Simpson,* N. A. Ahmed,† and R. D. Archer‡
University of New South Wales,
Kensington, New South Wales 2052, Australia

Introduction

THE flowfield in the tip region of a lifting wing is of great interest to the aircraft designer. This region of flow can have a strong influence on the performance of a wing and the production of induced drag. Efforts have been made over the years to reduce the induced drag associated with a lifting wing and to improve the overall lift-to-drag ratio by modifying the wing and the wingtip configuration.

One technique that has been the subject of several investigations is the use of pneumatic blowing outward from the wing tip. The active nature of such a technique offers the advantage that it can be utilized during the phases of flight at which it is best suited. Past efforts in analyzing the effect of blowing in the wing tip region have concentrated on flow visualization and flowfield measurements.[1–4] Some progress has been made toward identifying several aspects of the complex flow mechanisms, but more measurements of the global effects on the lift and drag of the wing are required.

This study looks at the overall lift and drag characteristics associated with blowing from the wing tip with a discrete planar jet exploiting the Coanda effect. The jet geometry has been designed to enhance the effect of blowing by vectoring the jet mass flow against the natural tip vortex. Comparisons involve variations in blowing coefficients and angles of attack at a constant Reynolds number.

Experiments

The test model shown in Fig. 1 is a rectangular wing of 300-mm chord with a half-span aspect ratio of 1.9 and with an NACA 0015 aerofoil section. The wing tip was designed as a body of revolution, and the jet outlet was faired into the shape to minimize the disturbances of the duct outlet geometry. The center of the Coanda jet was located at quarter chord and was 30 mm wide. Interchangeable tips were specifically designed to allow the change between the solid tip for the reference case and that of the Coanda jet.

The tests were performed in a closed circuit wind tunnel with a 1270×914 mm test section at a freestream speed of 25 m/s. The Reynolds number based on chord was 5.1×10^5. Freestream turbulence intensity was measured at 0.3%. A six-component balance was used to obtain the forces acting on the wing and a calibrated mass flow meter was used to determine the blowing coefficient of the Coanda jet. Standard wind-tunnel wall and blockage corrections were applied to the results.

Received 20 May 1999; revision received 16 July 1999; accepted for publication 27 July 1999.

*Graduate Student, Department of Aerospace Engineering.
†Senior Lecturer, Department of Aerospace Engineering.
‡Professor, Department of Aerospace Engineering.

Results and Discussion

Experiments were run for the reference case and the Coanda tip with blowing coefficients up to 0.01. The angle of attack ranged between 0 and 14 deg. For this study the blowing coefficient is defined as

$$C_\mu = \dot{m} V_j / q_\infty S$$

where $\dot{m}$ is the mass flow rate of the blowing jet (kilograms per second). V_j (meters per second) is the velocity of the jet, and q_∞ is the freestream dynamic pressure (pascal). S is the reference area (meters squared) taken as the planform area of the half-wing. Blowing coefficients tested fall in the range of those considered by other investigators.[1–4]

Lift Enhancement due to Blowing

It has been reported in other investigations[1–4] that a lifting wing experiences a lift enhancement due to spanwise blowing. In the study by Tavella and Roberts[2] simple scaling laws were derived to predict the effect of blowing on lift enhancement. This approach was based on perturbing the span of the wing by treating the jet as a thin momentum sheet subject to a pressure differential. The following equation was derived as a result[1]:

$$\Delta C_L / C_{Lo} = k_1 F(A)(C_\mu / \alpha)^{\frac{2}{3}}$$

where k_1 is a constant dependent on jet geometry and $F(A)$ is a function of aspect ratio. A comparison was made to assess the lift enhancement results obtained in this study to the most favorable jet geometry reported by Lee et al.[1] Figure 2 shows a comparison of these results. As can be seen from Fig. 2, the proposed scheme appears to be more effective than the jet configurations reported by Lee et al.[1]

Effects of Blowing on Aerodynamic Efficiency (Lift-to-Drag Ratio)

Figure 3 shows the lift-to-drag ratio for the wing without blowing and with a blowing coefficient of 0.01. Over the higher lift coefficients there is a distinct increase in the lift-to-drag ratio. For a C_L value of 0.8, the wing experiences an increase of about 6% in the lift-to-drag ratio for a C_μ of 0.01. In the lower C_L range (below 0.3) where induced drag is small compared to profile drag, the effects

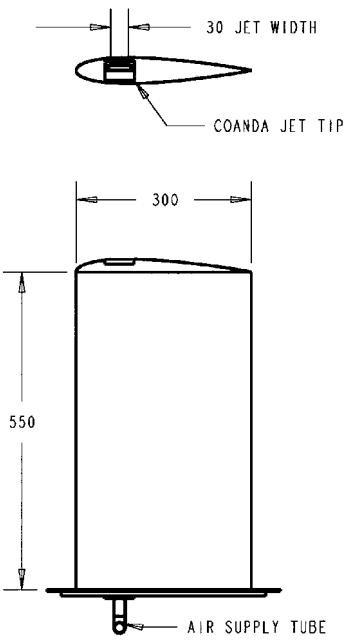

Fig. 1 Wing model, showing Coanda jet location.